Quantifying arrhythmic long QT effects of hydroxychloroquine and azithromycin with whole-heart optical mapping and simulations

Ilija Uzelac, PhD, MBA,[*1] Abouzar Kaboudian, PhD,[*1] Shahriar Iravanian, MD, MSE,[†] Jimena G. Siles-Paredes, MSc,[‡] James C. Gumbart, PhD,[*] Hiroshi Ashikaga, MD, PhD,[§] Neal Bhatia, MD, FHRS,[†] Robert F. Gilmour Jr., PhD,[‖] Elizabeth M. Cherry, PhD,[¶] Flavio H. Fenton, PhD[*]

*From the *School of Physics, Georgia Institute of Technology, Atlanta, Georgia, †Division of Cardiology, Section of Electrophysiology, Emory University Hospital, Atlanta, Georgia, ‡Universidad Privada del Valle, Santa Cruz, Bolivia, §Cardiac Arrhythmia Service, Johns Hopkins University School of Medicine, Baltimore, Maryland, ‖Biomedical Sciences, University of Prince Edward Island, Charlottetown, Canada, and ¶School of Computational Science and Engineering, Georgia Institute of Technology, Atlanta, Georgia.*

BACKGROUND In March 2020, hydroxychloroquine (HCQ) alone or combined with azithromycin (AZM) was authorized as a treatment for COVID-19 in many countries. The therapy proved ineffective with long QT and deadly cardiac arrhythmia risks, illustrating challenges to determine the new safety profile of repurposed drugs.

OBJECTIVE To investigate proarrhythmic effects and mechanism of HCQ and AZM (combined and alone) with high doses of HCQ as in the COVID-19 clinical trials.

METHODS Proarrhythmic effects of HCQ and AZM are quantified using optical mapping with voltage-sensitive dyes in ex vivo Langendorff-perfused guinea pig (GP) hearts and with numerical simulations of a GP Luo-Rudy and a human O'Hara-Virag-Varro-Rudy models, for Epi, Endo, and M cells, in cell and tissue, incorporating the drug's effect on cell membrane ionic currents.

RESULTS Experimentally, HCQ alone and combined with AZM leads to long QT intervals by prolonging the action potential duration and increased spatial dispersion of action potential (AP) repolarization across the heart, leading to proarrhythmic discordant alternans. AZM alone had a lesser arrhythmic effect with less triangulation of the AP shape. Mathematical cardiac models fail to reproduce most of the arrhythmic effects observed experimentally.

CONCLUSIONS During public health crises, the risks and benefits of new and repurposed drugs could be better assessed with alternative experimental and computational approaches to identify proarrhythmic mechanisms. Optical mapping is an effective framework suitable to investigate the drug's adverse effects on cardiac cell membrane ionic channels at the cellular level and arrhythmia mechanisms at the tissue and whole-organ level.

KEYWORDS Alternans; Action potential; Arrhythmias; Azithromycin; COVID-19; Cardiotoxic drugs; CiPA; Hydroxychloroquine; Optical mapping

(Heart Rhythm O^2 2021;2:394–404)

Introduction

The novel severe acute respiratory syndrome coronavirus 2 (SARS-CoV-2), which causes the coronavirus disease COVID-19, became a global pandemic in early 2020, generating a significant impact on public health. Given the time delays associated with developing a vaccine and new effective drugs, COVID-19 treatment modalities have relied on repurposed drugs such as remdesivir and dexamethasone, and hydroxychloroquine (HCQ) with azithromycin (AZM).

Based on positive in vitro studies[1,2] and a small nonrandomized study by Gautret and colleagues,[3] HCQ and its analog chloroquine (CQ) were authorized in many countries for off-label use to treat COVID-19 in March 2020. HCQ was included as 1 of the 4 drugs in the large international clinical trial SOLIDARITY organized by the World Health Organization. As evidence accumulated, the trials showed no benefit for HCQ/CQ with or without AZM and eventually were terminated, while also finding serious risk of the drug-induced long QT syndrome, leading to cardiac arrhythmia in some hospitalized patients.[4–8]

The key advantage of repurposed drugs is an established safety profile, and advancement to clinical trials and

[1]The first 2 authors contributed equally to this work. **Address reprint requests and correspondence:** Dr Ilija Uzelac, School of Physics, Georgia Institute of Technology, 837 State St, Atlanta, GA 30332. E-mail address: iuzelac3@gatech.edu.

2666-5018/

https://doi.org/10.1016/j.hroo.2021.06.008

KEY FINDINGS

- This study confirms that hydroxychloroquine (HCQ) and azithromycin (AZM) at high clinical concentrations leads to long QT intervals by prolonging the action potential duration (APD) and increased spatial dispersion of action potential (AP) repolarization across the heart, leading to proarrhythmic discordant alternans.
- HCQ and AZM are potentially arrhythmic as they increase the amplitude of alternans at shorter cycle length (CLs) and to move the onset of alternans toward higher CLs that are close and/or include CLs produced by the normal sinoatrial node.
- Most up-to-date, state-of-the-art mathematical models of cardiac cells (for guinea pig and human) failed in reproducing critical experimental data such as the development of APD alternans under simulated drug conditions.

applications can be expedited.[9] However, safety profiles need to be readdressed if new doses are higher and the patient population is different. This is even more important if comorbidities specific to the patient population are present. Before the COVID-19 pandemic, there were few reports of the proarrhythmic effects of HCQ, especially in combination with AZM. However, COVID-19 patients were treated using doses of an order of magnitude higher (6–12 g HCQ/CQ over 10 days[3,5]) than the standard HCQ dosage for malaria (310 mg base once per week). HCQ accumulates in cells, with a long half-life of approximately 50 days, and may lead to irreversible myocardial damage[10–12] at the higher concentrations used. Furthermore, COVID-19 itself can induce myocardial injury,[13–15] placing the general patient population at increased cardiovascular risk.[16] Therefore, HCQ/CQ's safety profile alone or in combination with AZM in COVID-19 patients can be significantly different from that for the malaria treatment. Because future pandemics are inevitable, there is an urgent need for an expedited framework, such as well-designed in vivo, ex vivo, and in vitro experiments, along with in silico models, to provide sufficient data regarding the safety and efficacy of repurposed drugs.

In this study, we present a detailed study of the effect of HCQ and AZM in whole-heart optical-mapping imaging and computer simulations. Our objectives were (1) to quantify, using optical mapping, the arrhythmogenic effects of HCQ and AZM on the action potential duration (APD) prolongation observed as QT interval prolongation on electrocardiograms (ECGs), spatial dispersion of APD observed as ECG T-wave alternans; and (2) to use numerical simulations using a guinea pig (GP) model to compare the effects of the drugs with experiments, and to help extrapolate the effects of these drugs to human hearts.

Methods

All procedures were approved by the Office of Research and Integrity Assurance at Georgia Institute of Technology in accordance with the provisions of the USDA Animal Welfare Act Regulations and Standards, PHS policy, conforming to the current Guide for Care and Use of Laboratory Animals. Materials and data that support the findings of this study are available from the corresponding author upon request. A detailed methods section can be found in the Data Supplement.

Briefly, we used optical-mapping imaging to elucidate the cellular proarrhythmic effects of HCQ and AZM in whole ex vivo arterially perfused GP hearts (n = 12). Drugs were added to the perfusate circulating through the isolated hearts, at 1 hour mark from the beginning of the experiment (heart cannulation), at concentrations equivalent to therapeutic serum doses of 1000 ng/mL (3.0 μM) for HCQ and 500 ng/mL (0.67 μM) for AZM. The hearts were stained with transmembrane potential (V_m)-sensitive fluorescent JPW-6003 dye for imaging of propagating electrical waves, represented as action potentials (APs) across the heart's surface at a high spatial and temporal resolution. (±)-Blebbistatin at a concentration of 1.8 μM was used as a contraction decoupler.[17] Sequences of fluorescence images were recorded using a high-speed EMCCD camera (Evolve 128, Photometrics) at resolution of 128 × 128 pixels (0.2 × 0.2 mm spatial resolution) at 500 Hz. AP repolarization was quantified as spatial and temporal dispersion of APD as a function of the stimulation period in restitution protocols.[18] Each experiment lasted 5–6 hours, and the time it took for drug effects to reach the plateau in the APD prolongation was around 2–3 hours after administration of the drugs or 3–4 hours from the beginning of the experiment. Restitution protocols were repeated every 30 minutes. As a control, we performed restitution protocols on 2 GP hearts with no drugs and confirmed that AP shape and APD restitution did not change from the beginning of the experiment to the end at the 6-hour mark. Similarly, at the beginning of all drug experiments we performed a restitution protocol before the drugs were added as control. Along with optical mapping, pseudo-ECGs (pECGs) were recorded from a pair of bipolar electrodes. To measure conduction velocity (CV), we used a 3-point measurement method (Supplemental Figure 1). The activation time at 3 noncollinear points (the vertices of a near isosceles triangle with a side length of 2 mm on the anterior aspect of the left ventricle) are used to measure CV, using a closed analytical formula (more details can be found in the Data Supplement).

For the numerical simulations, we used the most advanced ventricular cell model of GP heart,[19] and what is considered the state-of-the-art O'Hara-Virag-Varro-Rudy (OVVR) model[20] for human ventricular cells, in single cell and tissue using WebGL.[21] Simulations were carried out using explicit Euler for the voltage and a combination of Rush-Larsen and semi-implicit (backward Euler) for the gate variables[21,22] with time step of dt = 0.05 ms, and space discretization of dx = 150 μm in tissue-level simulations and the standard diffusion coefficient of 0.001 cm/ms^2. Tissue simulations

were performed in a 2-D isotropic monodomain with 1024 × 1024 cells (~15 cm^2). The area is chosen to be large enough to investigate the possibility of the development of concordant/discordant alternans. APD restitutions were obtained by stimulations induced at a corner of the 2-D domain to capture wavefront curvature effects.

Results

Experimental results

Before and after the addition of HCQ and AZM, we recorded pECGs (Figure 1A) and performed optical mapping of fluorescence signals to capture optical action potentials representing cellular V_m (Figure 1B). In the HCQ&AZM-treated hearts, pECG recordings showed QT prolongation at longer cycle lengths (CLs) along with pronounced T-wave alternans.[7,23,24] Similarly, in optical mapping recordings, we observed APD prolongation (the cellular mechanisms of QT prolongation) resulting in APD alternans (beat-to-beat variations in APD, and cellular mechanism of T-wave alternans). Additionally, we observed spatial APD dispersion.[24,25] APD was calculated at 75% repolarization of AP, unless otherwise noted, and spatial distribution maps of APD were calculated across the whole anterior heart surface (Figure 1C). Before the drugs were added, the APD maps showed no change in the APD dispersion between even and odd beats. As expected in healthy hearts, as the CL decreased, the APD decreased, but the spatial distribution of APD did not change. However, infusion of HCQ&AZM increased the spatial dispersion of APD, as indicated by the higher maximum APD values across all CLs and lower minimum APD values at short CLs compared to the control restitution measurements with no drugs. The effects of the drugs was to increase the amplitude of alternans at shorter

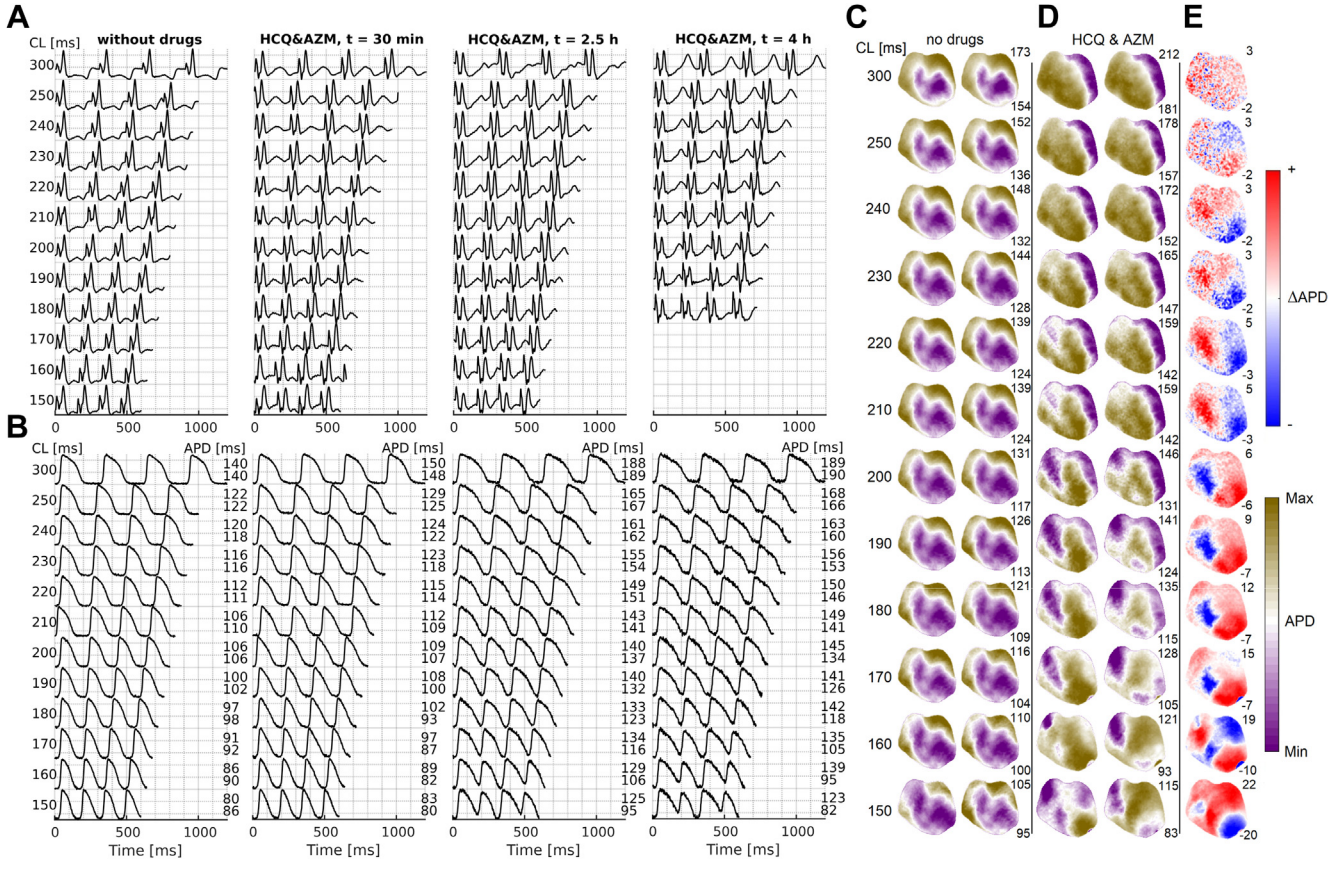

Figure 1 Arrhythmic effects after application of hydroxychloroquine plus azithromycin (HCQ&AZM). **A:** Guinea pig electrocardiogram (ECG) before the drugs were added for different periods of stimulation; cycle lengths (CLs), from 300 ms to 150 ms, indicated by the numbers in the left and at different times (columns) during the experiment, counting from the time when the HCQ&AZM drugs were added. After 2.5 hours the action potential duration (APD) changes have reached a plateau and did not change significantly later on during the experiment. The ECG shows what would appear as 2 QRS complexes. The first is the stimulation electrode's stimulus artifact, followed by the actual QRS indicating the heart's activation and the T wave indicating its deactivation. There is a clear QT prolongation under HCQ&AZM, in addition to T-wave alternans (TWA). **B:** The optical action potential (AP) signal from 1 pixel, showing the cellular mechanism of QT prolongation and TWA. Under HCQ&AZM, the APD prolongs, and there is the development of period 2 alternans, alternating short and long APDs at shorter CLs. Alternans is absent without the drugs. **C-D:** Spatial distribution of APD across the tissue for even and odd beats as a function of the pacing period of stimulation before and after HCQ&AZM. Before the drugs were added, the same pattern for even and odd beats indicate no increase in spatial APD dispersion. However, with HCQ&AZM, we observed APD dispersion that further develops as the stimulation period decreases, creating an increased susceptibility for arrhythmia. Numbers to the right indicate 3rd and 97th percentile of APD values, expressed for each CL. **E:** Blue-red patterns show variations in APD (ΔAPD) between even and odd beats, showing a transition from no alternans to concordant alternans and then into discordant alternans clearly forming for CLs under 180 ms.

CLs and to move the onset of alternans toward higher CLs. In Figure 1C, concordant alternans are already present at CL = 300 ms and transform into spatially discordant alternans around a CL of 220 ms. Below a CL of 160 ms, multiple spatially discordant alternating regions develop. In the HCQ-alone- and AZM-alone-treated hearts, we observed APD prolongation at longer CLs with increased alternans amplitude at shorter CLs (Supplemental Figure 2).

The effects of HCQ, AZM, and HCQ&AZM on APD prolongation across all 12 experiments were compared (Table 1) using the maximum (extrapolated) APD values (APDlim, the maximal APD values from the restitution fit curves at longer CLs), and the APDs measured at CL of 250 ms. CL of 250 ms was chosen as the natural sinoatrial CL for GPs. The reported APD values represent the mean from optical APs from 15 spatially distributed points on the left ventricle's epicardial surface. HCQ, alone or combined with AZM, significantly prolonged APD (Figure 2 and Supplemental Figure 2), creating a substrate for arrhythmias with increased APD spatial dispersion (Figure 1C–E). In HCQ&AZM-treated hearts, the APD increased from 138.0 ± 3.9 ms to 162.2 ± 7.1 ms (P = .02). APD prolongation was more pronounced in the HCQ-treated hearts, in which APD increased from 132.4 ± 1.2 ms to 176.7 ± 6.1 ms (P < .01). In AZM-treated hearts, AZM had a modest effect on APD with no statistically significant difference (127.1 ± 17.9 ms to 152.1 ± 13.7 ms, P = .26). There was no statistically significant APD prolongation (P = .14) in the control experiments during the entire course of the experiments exceeding 6 hours (Table 1 and Figure 2).

Alternans occur during cardiac cell repolarization and develop in cardiac tissue at short periods of stimulation.[18,24] The magnitude of repolarization alternans can vary across heart tissue, causing spatial dispersion of repolarization and forming a substrate for the initiation of reentrant arrhythmias.[18,24–26] GP hearts are not specifically vulnerable to alternans even at fast pacing rates and temperature has to be decreased to elicit alternans.[24]

We defined the CL at the onset of alternans (ACL) as the CL at which alternans exceed 5 ms across at least 5% area of the imaged ventricles. In the control experiments, ACL at the beginning of the experiments and after 6 hours were 150 ms and 145 ± 5 ms, respectively (Table 2), indicating no significant change in heart electrophysiology. Furthermore, for each experiment with the drugs, we first performed 2 restitution recordings before adding the drug(s). We observed that alternans developed in the drug-treated hearts at normal body temperature and, more importantly, even at physiological CLs for GPs (Table 2, Figure 1B, and Supplemental Figure 2). Table 2 shows that only half of the GPs developed alternans before administering the drugs, and the average ACL when alternans developed was 147 ± 16 ms. However, in all isolated GP hearts treated with HCQ, AZM, or HCQ&AZM, alternans developed at higher CLs. The mean ACL was 211.7 ± 11.9 ms (P < .01) for the HCQ&AZM-treated hearts, 185 ± 45 ms for AZM hearts, and 245 ± 35 ms for HCQ hearts (P < .01). P values are calculated by performing t tests on ACLs before and after the drugs were given.

Table 1 Summary values from all 12 experiments and averages for control, hydroxychloroquine, azithromycin, and hydroxychloroquine plus azithromycin for action potential duration and conduction velocity measurements

#	Group	$APD250_b$ [ms]	$APD250_a$ [ms]	$APDlim_b$ [ms]	$APDlim_a$ [ms]	CV_b [cm/s]	CV_a [cm/s]
1	Control	138.9 ± 0.5	152.4 ± 0.6	197.1 ± 7.7	177.9 ± 6.7	57.4 ± 0.4	69.5 ± 0.9
2	Control	126.3 ± 0.8	141.2 ± 0.6	175.8 ± 4.3	172.8 ± 8.9	78.7 ± 0.5	65.9 ± 0.5
3	HCQ	131.6 ± 0.7	181.3 ± 2.1	166.2 ± 2.7	311.0 ± 39.0	52.7 ± 0.2	36.6 ± 0.4
4	HCQ	133.1 ± 0.7	172.1 ± 3.5	185.0 ± 10.0	261.0 ± 27.0	85.2 ± 0.9	89.4 ± 1.4
5	AZM	145.0 ± 0.5	164.7 ± 3.4	183.6 ± 5.3	229.0 ± 19.0	58.9 ± 0.2	56.3 ± 1.1
6	AZM	109.2 ± 0.6	139.4 ± 3.9	130.4 ± 6.5	175.0 ± 25.0	69.9 ± 0.4	49.2 ± 0.6
7	HCQ&AZM	143.1 ± 0.9	187.8 ± 2.7	157.5 ± 6.6	300.0 ± 26.0	38.9 ± 0.4	49.5 ± 1.4
8	HCQ&AZM	134.0 ± 0.4	163.7 ± 0.9	162.7 ± 7.6	240.0 ± 19.0	62.6 ± 0.3	49.7 ± 0.3
9	HCQ&AZM	145.0 ± 0.4	159.1 ± 2.5	201.3 ± 4.5	273.0 ± 33.0	59.4 ± 0.2	55.7 ± 0.9
10	HCQ&AZM	131.8 ± 0.7	143.1 ± 2.3	200.0 ± 11.0	190.0 ± 24.0	67.6 ± 0.5	73.5 ± 1.1
11	HCQ&AZM	148.0 ± 0.6	158.6 ± 1.1	216.0 ± 11.0	309.0 ± 17.0	72.9 ± 0.3	68.3 ± 0.7
12	HCQ&AZM	125.9 ± 0.6	160.6 ± 2.0	205.0 ± 13.0	216.0 ± 14.0	48.0 ± 0.2	49.5 ± 0.5

	$APD250_b$ [ms]	$APD250_a$ [ms]	P value	$APDlim_b$ [ms]	$APDlim_a$ [ms]	P value	CV_b [cm/s]	CV_a [cm/s]	P value
Control	132.6 ± 6.4	146.8 ± 5.7	.14	186.5 ± 13.8	175.4 ± 5.7	.40	68.1 ± 10.7	67.7 ± 2.1	.96
HCQ	132.4 ± 1.2	176.7 ± 6.1	<.01	175.6 ± 14.0	286.0 ± 35.4	.05	69.0 ± 16.3	63.0 ± 26.4	.82
AZM	127.1 ± 17.9	152.1 ± 13.7	.26	157.0 ± 27.9	202.0 ± 31.8	.27	64.4 ± 5.5	52.8 ± 3.8	.13
HCQ&AZM	138.0 ± 3.9	162.2 ± 7.7	.02	190.4 ± 25.1	254.7 ± 24.4	<.01	58.2 ± 5.2	57.7 ± 4.9	.87

Subscript b/a indicates before and after drug treatment. The "before" measurements are performed 30–45 minutes into the experiment before any drug has been added (around 1 hour experiment mark); "after" refers to measurements obtained once measured values reached steady state, typically 2–3 hours after the drugs were added.

P value represents the P value for the difference between the 2 prior columns.

APD250 = action potential duration calculated at 75% repolarization of action potential (APD_{75}), at pacing cycle length (CL) of 250 ms (physiological/natural CL for guinea pigs); APDlim = the estimated limit value of APD_{75}) based on the restitution curve at large CLs; AZM = azithromycin; CV = the average conduction velocity in cm/s for CL of 250 ms; HCQ = hydroxychloroquine.

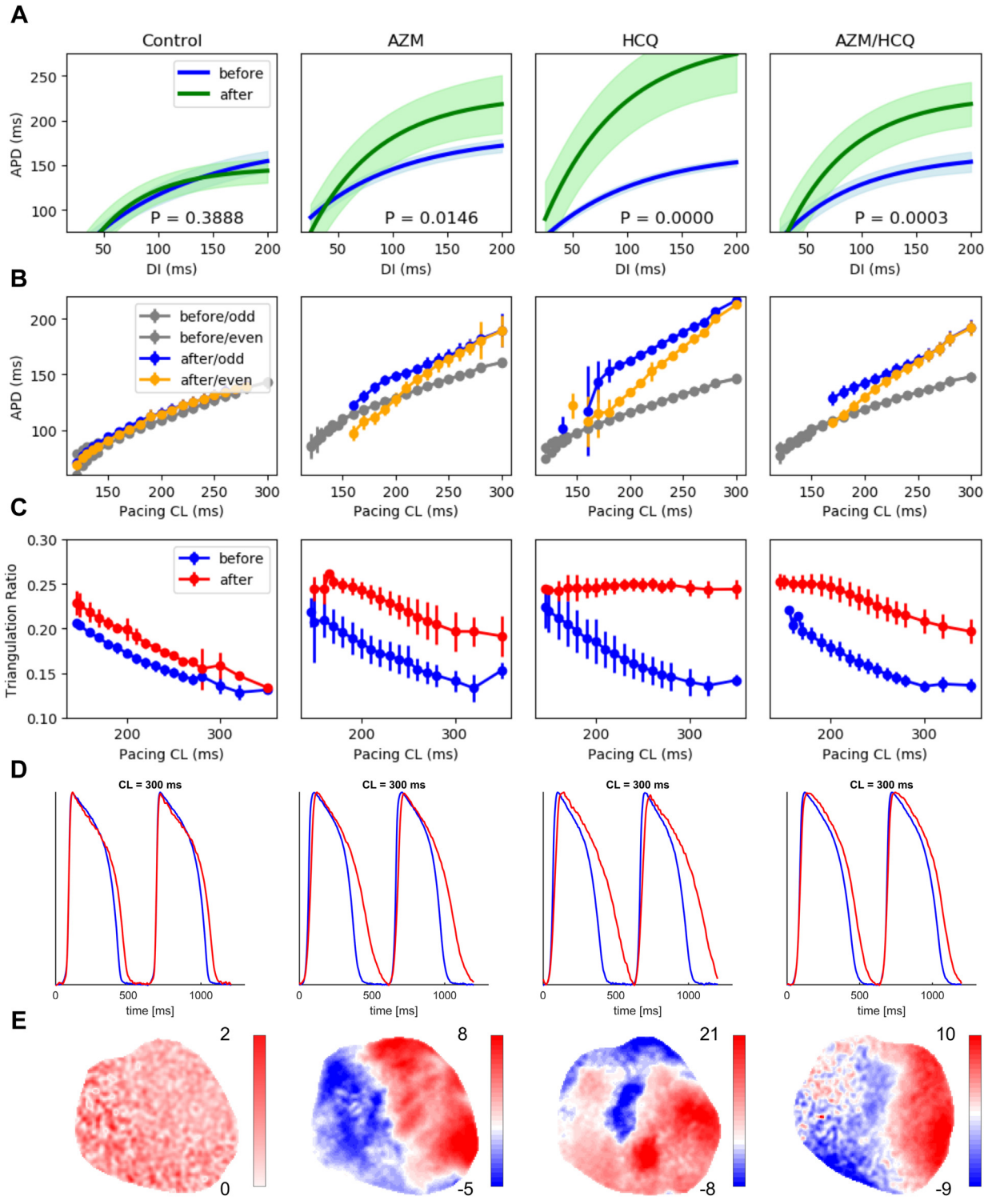

Figure 2 Quantifying effects of azithromycin (AZM), hydroxychloroquine (HCQ), and AZM&HCQ as a function of pacing cycle length (CL). **A:** The restitution curves, depicting the steady-state action potential duration (APD) vs the diastolic interval, averaged across 15 spatially distributed points over the left ventricular epicardial surface for 4 different treatments. In control experiments, the blue restitution curve is obtained at the beginning of experiments and the green curves are after 6 hours. In drug-treated hearts, the blue curves show the untreated control curves obtained at the beginning of the experiment, and the green curves are after APD prolongation reached plateau, 2–3 hours after drugs administration. The shaded areas indicate 95% confidence interval of the fit. **B:** APD steady-state curves vs pacing cycle length (period) obtained before (gray) and after (yellow: even beats, blue: odd beats) infusion of the drugs for the same 15 points as in **A**. **C:** Action potential (AP) triangulation ratio as a function of the period of stimulation before (blue) and after (red) infusion of the drugs. The triangulation index was calculated across the entire imaged portion of the epicardial surface of the left ventricle and increased at longer stimulation periods in the HCQ and HCQ&AZM groups. **D:** Optical AP traces obtained at a CL = 250 ms, from a single pixel on the left ventricle, showing APD prolongation in the drug groups. Note the triangular shape of the HCQ- and HCQ&AZM-treated APs. **E:** APD dispersion maps for CL = 180 ms, showing no alternans for control, and discordant alternans for AZM, HCQ, and AZM&HCQ.

Table 2 Summary values from all 12 experiments and averages for control, hydroxychloroquine, azithromycin, and hydroxychloroquine plus azithromycin for alternans measurements

#	Group	ACL_b [ms]	ACL_a [ms]	Alt_b [ms]	Alt_a [ms]	$Slope_b$	$Slope_a$	DI_b	DI_a
1	Control		140		28.4		1.34 ± 0.08		35.8 ± 2.9
2	Control	150	150	12.2	11.1	0.90 ± 0.09	1.15 ± 0.09	61.0 ± 2.7	51.5 ± 3.7
3	HCQ	130	280	8.3	30.6	0.90 ± 0.03	1.42 ± 0.11	42.7 ± 3.3	78.3 ± 3.3
4	HCQ	160	210	9.9	10.1	0.92 ± 0.05	1.63 ± 0.01	61.4 ± 3.3	57.5 ± 4.9
5	AZM		230		28.1		1.16 ± 0.09		71.5 ± 6.5
6	AZM		140		10.4		1.54 ± 0.19		51.9 ± 6.9
7	HCQ&AZM		240		11.7		1.58 ± 0.11		65.3 ± 3.8
8	HCQ&AZM	126	250	6.1	20.0	1.04 ± 0.04	1.24 ± 0.07	40.9 ± 4.0	83.6 ± 3.0
9	HCQ&AZM		200	10.7	14.0		1.37 ± 0.07		66.1 ± 3.3
10	HCQ&AZM	180	200	7.2	21.1	0.98 ± 0.05	1.14 ± 0.08	75.6 ± 5.5	78.2 ± 4.3
11	HCQ&AZM	130	170	7.2	15.2	1.02 ± 0.14	1.42 ± 0.16	43.0 ± 4.8	51.6 ± 4.2
12	HCQ&AZM		210		25.2		1.15 ± 0.05		66.2 ± 3.9

	ACL_b [ms]	ACL_a [ms]	*P* value	Alt_b [ms]	Alt_a [ms]	*P* value	$Slope_b$	$Slope_a$	*P* value
Control	150.0	145.0 ± 5.0	N/A	12.2	19.8 ± 8.7	N/A	0.90	1.25 ± 0.10	N/A
HCQ	145.0 ± 15.0	245.0 ± 35.0	<.01	9.1 ± 0.8	20.4 ± 10.3	.26	0.91 ± 0.01	1.53 ± 0.11	.02
AZM		185.0 ± 45.0	N/A		19.3 ± 8.9	N/A		1.35 ± 0.19	N/A
HCQ&AZM	145.3 ± 17.4	211.7 ± 11.9	<.01	7.8 ± 1.0	17.9 ± 2.1	<.01	1.01 ± 0.02	1.32 ± 0.07	<.01

Subscript b/a indicates before and after drug treatment. The "before" measurements are performed 30–45 minutes into the experiment before any drug has been added (around 1 hour experiment mark); "after" refers to measurements obtained once measured values reached steady state, typically 2–3 hours after the drugs were added.

P value represents the *P* value for the difference between the 2 prior columns.

ACL = cycle length (CL) at the onset of alternans exceeding 5 ms in amplitude over 5% of greater tissue area (no value indicates no alternans was present); Alt = maximum alternans amplitude between even and odd beats (ms); AZM = azithromycin; DI = diastolic interval at the onset of alternans (ms); HCQ = hydroxychloroquine; Slope = the slope of the action potential duration restitution curve at the onset of alternans.

To further quantify the effects of the drugs on APD prolongation across a broad range of pacing CLs, we calculated restitution curves, APD vs diastolic interval (DI), and triangulation ratios. DI is the time from the end of an AP to the next AP's upstroke such that CL = APD + DI. We used 75% of repolarization as the threshold to separate APD from DI. Restitution curves were fitted to a single exponential curve from data of 15 selected pixels across the left ventricle (Supplemental Table 1). Figure 2A shows the averaged restitution curves for the 4 different treatments. HCQ, AZM, and HCQ&AZM shifted the restitution curves upward, consistent with the differences in APD250 values (Table 1). Additionally, the slopes of the restitution curves in drug-treated hearts increased (Table 2). For HCQ&AZM-treated hearts, the restitution curve slope at the onset of alternans increased from 1.01 ± 0.02 to 1.32 ± 0.07 ($P < .01$), and the alternans amplitude increased as well (17.9 ± 2.1 ms vs 7.8 ± 1.0 ms, $P < .01$). The effect of AZM on the restitution curve was less than HCQ and HCQ&AZM. HCQ alone resulted in the restitution curve shift more than HCQ&AZM, APDlim = 286.0 ± 35.4 ms vs 254.7 ± 24.4 ms (Table 1).

AZM, HCQ, and HCQ&AZM predominantly affected the repolarization phase and did not have a major effect on CV (Table 1). While HCQ alone blocks sodium channels across the cell membrane the mean CV at CL = 250 ms did not change significantly after HCQ&AZM treatment ($P < .87$), 57.7 ± 4.9 cm/s compared to 58.2 ± 5.2 cm/s with no drugs added. This is expected, as the relation of CV with sodium channels conductance is not linear with nonuniform distribution of sodium channels, and it has been shown not to be proportional to the maximum upstroke velocity.[27] In numerical models, CV has been shown to depend on the overall integral of the upstroke, the threshold of excitation, and nonuniform distribution of sodium channels, among other parameters.

Modeling results

Numerical simulations using a detailed cardiac cell model for GP ionic currents[19] were performed in single cell and in tissue to compare with experiments. The simulation results were then extrapolated to a human ventricular model using the OVVR model in 3 different cell types (Epi, Endo, and M cell) in single cell and in tissue).[20] The GP model was rescaled to match the experimental data (as the model's APD is shorter than APD in the control experiments at physiological CLs). We modeled the effects of HCQ and AZM by reducing ionic currents following pharmacological data.[28] Briefly, based on ion channel voltage-clamp studies,[28–30] the effects of HCQ were simulated by reducing the sodium current (I_{Na}) up to 25% ± 4%, the rapid delayed rectifier potassium current (I_{Kr}) by up to 65% ± 7%, and the slowly activating potassium currents (I_{Ks}) by up to 7% ± 6%, and inwardly rectifying potassium current (I_{K1}) by 35% ± 7% (but we tested to up to 85% as in[28]), and lastly, the L-type channel was blocked by up to 9% ± 3%, which affects the L-type calcium current (I_{CaL}), sodium current (I_{CaNaL}), and potassium current (I_{CaKL}) as well. The magnitudes of reduction in ionic currents in our simulations are well within the experimentally observed values in HCQ- and AZM-treated hearts and the

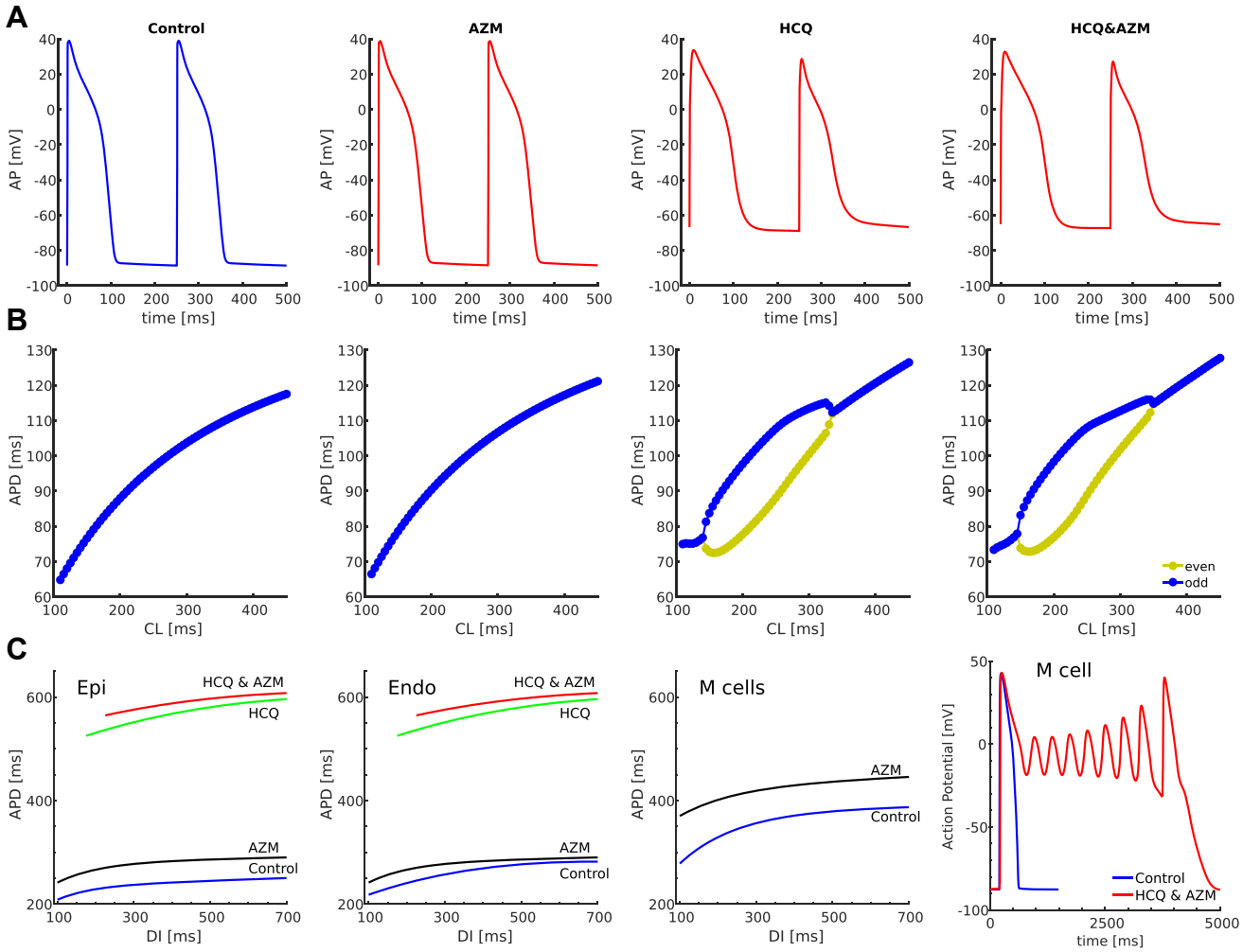

Figure 3 Numerical results. **A:** Action potential shapes were obtained in the guinea pig (GP) mathematical cell model for control, azithromycin (AZM), hydroxychloroquine (HCQ), and HCQ&AZM. The GP models replicate alternans and prolongation of the action potential (AP) repolarization phase under HCQ and HCQ&AZM, as in the experimental observations. However, the resting membrane potential is elevated. **B:** AP restitution curves showing alternans from beat to beat for simulations that include the drug effects of HCQ and HCQ/AZM. The GP model fails to replicate alternans during control at cycle lengths (CLs) < 150 ms and under AZM at physiological CLs. **C:** AP duration restitution curves before and after drugs in the O'Hara-Virag-Varro-Rudy (OVVR) human ventricle model for Epi, Endo, and M cells, obtained from pacing in simulated 2-D tissue, at a corner and measured in the center of the tissue model. The restitution curves are plotted across physiological heart rates. No restitution curves are shown for the M cell under HCQ and HCQ&AZ, as they produced early afterdepolarizations that propagated in tissue. The GP and OVVR models, in their current form, are not able to reproduce the dynamics of the experiments quantitatively and may require revision using robust experimental data.

theoretical values calculated using the Hill's equation from the in vitro measurements of half-maximal inhibitory concentrations of HCQ and AZM when applied to different ionic channels.[28]

For the GP model, AZM only slightly prolonged APD, which was less than in the experiments (Figure 2D, Supplemental Figure 2, Figure 3A, and Supplemental Figure 3). Consistent with experimental observations (Figure 2D and Supplemental Figure 2), HCQ prolonged APD in single-cell simulations, such that APD alternans developed at physiological CLs (Figure 3A and Supplemental Figure 3). Alternans was suppressed in simulations performed at the tissue level, with a slight reduction in maximum APD. However, the elevation of the resting membrane potential in simulations seems to be a significant discrepancy from the experiments (Figure 3A, and Supplemental Figure 3). Although measurement of the resting membrane potential with V_m-sensitive dyes is difficult, the large increase in resting membrane potential in the simulations should substantially decrease the amplitude of the signal, something that was not observed experimentally. The combination of AZM and HCQ further prolonged APD and slightly increased the range of CLs causing alternans. Maps of activation wavefronts and repolarization wavebacks are shown in Supplemental Figure 4, illustrating the change in morphology and direction under HCQ&AZM as long QT increases and repolarization alternans appears.

Simulations in the OVVR human model, both in single cell and tissue, showed that AZM, HCQ, and HCQ&AZM prolong APD significantly more than observed experimentally in HCQ&AZM-treated hearts of GP. The QT-prolonging effects were obvious for the Epi and Endo type cells

(Figure 3C). However, for the M cell types, HCQ and HCQ&AZM led to easy inducibility of runs of early afterdepolarizations (EADs) (Figure 3C), even after a first stimulus starting from resting initial conditions. Therefore, APD restitution curves could not be measured for the M cells, and APDs with EADs lasted almost 5 seconds, which is unphysiological. Furthermore, no alternans was observed in any of the cell types under the drugs. The human model did not display the elevated resting membrane potential as the GP model did. For the human model, blocking of I_{K1} to up to 85% had no statistical effect on the APD or resting membrane potential.

Our numerical simulations for the effects of AZM, HCQ, and AZM&HCQ on the human model agree with the overall results obtained in the study of Delaunois and colleagues,[28] using the OVVR model and its 2 variations. The study considered some population cell variations, a control "healthy" population of ~400 cells, and a "high-risk population" of ~100 cells. However, simulations were performed only in a single cell, a model of the epicardial cell, and only for 1 pacing CL of 1 second. Their results also showed APD prolongation, but no alternans was reported and no APD repolarization irregularities for AZM, HCQ, and AZM&HCQ at concentrations equivalent to therapeutic serum doses of HCQ and AZM used for COVID-19 in hospitalized patients. AP repolarization abnormalities were found only at unrealistic high values of 100, 300, and 1000 μM of HCQ concentrations, corresponding to 33, 100, and 333 times the values used in the clinical trials and our experiments, which are an order of magnitude higher than the highest clinical uses.

Discussion

We found that in GP hearts, HCQ combined with AZM leads to QT prolongation, in agreement with previous clinical studies.[7] Furthermore, using optical mapping technique, we linked the QT interval prolongation not only to an increase in the APD at the cellular level but also to spatial dispersion of AP repolarization. In the GP hearts treated with HCQ&AZM, the QT was prolonged at a physiological heart rate of 250 ms. At shorter CLs, APD alternans and dispersion occurred, and the surface of ventricles was divided into multiple regions based on the phase of the APD. The spatial APD dispersion led to spatially discordant alternans (Figure 1C), which is the cellular equivalent of T-wave alternans in the pECG (Figure 1A), a clinical marker for arrhythmia susceptibility and risk of sudden cardiac death.[31,32] Importantly, in GP control hearts without drugs, there was no increase in the dispersion of AP repolarization over the range of pacing CLs from 300 ms down to 150 ms (Figure 2A and Table 1).

Antibiotics such as erythromycin often prolong the QT interval by blocking the hERG potassium channel, resulting in slower cardiac repolarization and an increased risk of fatal arrhythmia. However, not all QT interval prolongations are proarrhythmic. For instance, AZM has a low affinity for the hERG channel[33] and prolongs the QT interval in a manner that does not seem to increase the risk of arrhythmia.[34] In addition to APD prolongation and APD restitution curve shift, APD triangulation is another important arrhythmic indicator,[35–37] expressed as $(APD_{75} - APD_{30})/CL$ (Figure 2C).[37] Lower triangulation ratios with AZM and AZM&HCQ manifest as the lengthening of the plateau phase (phase II of AP) in addition to the repolarization phase lengthening (phase III), which is observed at physiological CLs of above 200 ms (Figure 2D and Supplemental Figure 2). This may explain the lower incidence of alternans in AZM- and HCQ&AZM-treated hearts with smaller ACL value than in HCQ-treated hearts (Table 2 and Figure 2B). HCQ prolongs APD predominantly owing to prolongation of the AP repolarization phase (Figure 2D), resulting in a higher triangulation ratio (Figure 2C) than AZM and HCQ&AZM. A larger triangulation ratio has been shown previously to be associated with increased susceptibility to alternans[36] and formation of EADs.[38,39] Alternans and EADs are known factors in developing torsade de pointes[40–42] leading to deadly ventricular fibrillation. Lower triangulation ratios with HCQ&AZM compared to HCQ alone (Figure 2C) and lower ACLs (Table 2 and Figure 2B) are in agreement with a recent clinical study where the QT interval was shorter in the HCQ&AZM combo-treated patients compared to HCQ alone.[43] These findings show that APD prolongation mechanisms of HCQ and AZM are not additive, and we hypothesize that proarrhythmic effects of HCQ can be counteracted to a certain degree with drugs such as AZM that prolong the plateau phase of AP.

Both AZM and HCQ block predominantly delayed rectifier potassium channels in the cell's membrane, leading to APD prolongation in the AP repolarization phase. Since GP and humans have similar distributions of these channels,[44,45] GP is a commonly used model to test drug-induced repolarization abnormalities that could affect humans.[46–48] We used the GP mathematical model for cardiac cells from Livshitz and Rudy[19] to incorporate experimental observations. The same model changes were extrapolated to the 3 cell types of the human OVVR[20] ventricular cardiac model, recognized as the gold standard to study drug effects by the Comprehensive in Vitro Proarrhythmia Assay (CiPA) initiative,[49] sponsored by the Food and Drug Administration.

The numerical simulations with the GP model in single cell reproduced APD prolongation and development of alternans with HCQ alone and HCQ&AZM. However, the GP model did not reproduce the magnitudes of APD alternans and the CL for the onset of APD alternans. Furthermore, the model showed almost no effect of AZM alone, and simulations in tissue exhibited no significant alternans. Using the human ventricular model in a single cell and in tissue, we observed APD prolongation with HCQ, as predicted by the GP model (Figure 3 and Supplemental Figure 3), as consistent with clinical data.[7] However, unlike in the GP model, no alternans developed in the human model even for the single cell simulation in 3 different cell types (Epi, Endo, M

cells). This is not unexpected because the OVVR model has limitations to reproduce alternans compared to clinical studies.[50]

Human *in silico* models of cardiac tissue with the ability to reproduce the drug response in membrane ionic channels would be a significant step towards studying and understanding the arrhythmia mechanisms of drugs. However, the current models remain limited, as the models are often optimized to reproduce a particular experimental observation. Additionally, model parameters are typically obtained from a mix of data ranging from different experimental setups and animal species. Modification of an *in silico* model to study adverse drug effects *in silico* is a challenging task. Clinical trials with *in silico* models have been identified by CiPA as an alternative to the traditional drug approval process, representing an ongoing shift from traditionally empirical evidence towards the understanding of adverse effects on the ionic channels and their role in arrhythmogenesis. However, this study shows that even the most complete heart models do not accurately characterize the effects of different drugs on ionic membrane currents. This creates an even greater challenge for integrating the cell models into more complex 3-D heart models, and current CiPA drug modeling guidance needs to be modified to overcome the current challenges.

Conclusion

In summary, we have presented protocols used in ex vivo experiments and computer simulations that can be used to investigate the adverse effects of new or repurposed drugs on cardiac ionic channels at the cellular and tissue levels. Until recently, optical mapping systems required expensive high-speed cameras, not widely affordable for basic researchers. However, with advents in technology, these cameras are now becoming more affordable.[51] Similarly, until recently, simulations of complex cardiac models were limited to research groups with access to supercomputers, but the development of graphical processing units with thousands of computational cores and programs designed to exploit them have enabled simulations of these complex models, including computationally expensive parameter-fitting simulations, to be performed easily and efficiently using local PC workstations.[21] With optical-mapping imaging, we investigated the proarrhythmic effects of HCQ and AZM, 2 drugs rarely used together before and, for HCQ, used at much higher concentration to treat COVID-19 than their intended purpose, raising questions about new safety profiles. We have found that temporal APD prolongation and spatial dispersion of APD alternans are the mechanisms responsible for QT prolongation, a known proarrhythmic surrogate in clinical practice. Although numerical simulations can provide information on how the drugs directly affect the ion currents to a certain level, our results show that the current models lack the accuracy needed for quantitatively predictive studies. Therefore, caution is still required when interpreting results from computational models used to study drug cardiotoxicity.

Limitations of the study

Arrhythmia susceptibility owing to drug-induced APD prolongation is based on the amount of repolarization reserve, the ratio of I_{Kr} to I_{Ks} current, which varies significantly across mammalian species. In GP hearts,[52] the ratio of I_{Kr} to I_{Ks} is $\sim$10:1, whereas in human hearts[53] it is $\sim$1:3. As HCQ primarily blocks I_{Kr} channels, the same drug concentrations would be expected to lead to significantly less pronounced APD prolongation in humans than in GP hearts. However, other mechanisms may play a role, as drug-induced partial blockage of I_{Kr} channels may lead to overexpression of I_{K1} and I_{Ks} repolarization currents. Hence, a direct comparison is not straightforward. Nevertheless, GP and rabbits are species commonly used to test for drug-induced repolarization abnormalities that could affect humans.[46,47] We did not investigate if HCQ and/or AZM interact with the voltage-sensitive dye and/or blebbistatin used in this study. Numerically we only studied the effect of the drugs on the maximum conductance of the currents, and it may be of interest to investigate how the binding/unbinding rate constants of the drugs with cell membrane ionic channels are affected by different drugs concentrations, membrane voltage potential, and stimulation frequency using, for example, the modulated receptor method.[54,55] We chose the OVVR model over other existing human ventricular cell models, as it is the model designated by CiPA to investigate numerically drugs' arrhythmic effects.

Funding Sources

This study was supported by grants NIH 1R01HL143450-01, National Science Foundation 1446675, National Science Foundation CNS-2028677, and National Science Foundation Physics of Living Systems 1806833 (Drs Uzelac, Kaboudian, Gumbart, Cherry, and Fenton).

Disclosures

Dr Uzelac is the owner of Aleksa Tech. All other authors report no relevant conflicts of interest or disclosures.

Authorship

All authors attest they meet the current ICMJE criteria for authorship.

Patient Consent

Human subjects were not used in this study.

Ethics Statement

All procedures were approved by the Office of Research and Integrity Assurance at Georgia Institute of Technology in accordance with the provisions of the USDA Animal Welfare

Act Regulations and Standards, PHS policy, conforming to the current Guide for Care and Use of Laboratory Animals.

Appendix

Supplementary data

Supplementary data associated with this article can be found in the online version at https://doi.org/10.1016/j.hroo.2021.06.008.

References

1. Wang M, Cao R, Zhang L, et al. Remdesivir and chloroquine effectively inhibit the recently emerged novel coronavirus (2019-NCOV) in vitro. Cell Res 2020; 30:269–271.
2. Yao X, Ye F, Zhang M, et al. In vitro antiviral activity and projection of optimized dosing design of hydroxychloroquine for the treatment of severe acute respiratory syndrome coronavirus 2 (SARS-CoV-2). Clin Infect Dis 2020;71:732–739.
3. Gautret P, Lagier JC, Parola P, et al. Hydroxychloroquine and azithromycin as a treatment of COVID-19: results of an open-label non-randomized clinical trial. Int J Antimicrob Agents 2020;56:105949.
4. Molina JM, Delaugerre C, Le Goff J, et al. No evidence of rapid antiviral clearance or clinical benefit with the combination of hydroxychloroquine and azithromycin in patients with severe covid-19 infection. Med Mal Infect 2020; 50:384.
5. Borba MGS, Val FFA, Sampaio VS, et al. Effect of high vs low doses of chloroquine diphosphate as adjunctive therapy for patients hospitalized with severe acute respiratory syndrome coronavirus 2 (SARS-CoV-2) infection: a randomized clinical trial. JAMA Netw Open 2020;3:e208857–e208857.
6. Mercuro NJ, Yen CF, Shim DJ, et al. Risk of QT interval prolongation associated with use of hydroxychloroquine with or without concomitant azithromycin among hospitalized patients testing positive for coronavirus disease 2019 (COVID-19). JAMA Cardiol 2020;5:1036–1041.
7. Chorin E, Dai M, Shulman E, et al. The QT interval in patients with COVID-19 treated with hydroxychloroquine and azithromycin. Nat Med 2020; 26:808–809.
8. Cavalcanti AB, Zampieri FG, Rosa RG, et al. Hydroxychloroquine with or without azithromycin in mild-to-moderate COVID-19. N Engl J Med 2020; 383:2041–2052.
9. Oprea TI, Overington JP. Computational and practical aspects of drug repositioning. ASSAY Drug Dev Techn 2015;13:299–306.
10. Chatre C, Roubille F, Vernhet H, Jorgensen C, Pers YM. Cardiac complications attributed to chloroquine and hydroxychloroquine: a systematic review of the literature. Drug Saf 2018;41:919–931.
11. Joyce E, Fabre A, Mahon N. Hydroxychloroquine cardiotoxicity presenting as a rapidly evolving biventricular cardiomyopathy: key diagnostic features and literature review. Eur Heart J 2013;2:77–83.
12. Soong TR, Barouch LA, Champion HC, Wigley FM, Halushka MK. New clinical and ultrastructural findings in hydroxychloroquine-induced cardiomyopathy—a report of 2 cases. Hum Pathol 2007;38:1858–1863.
13. Lai CC, Shih TP, Ko WC, Tang HJ, Hsueh PR. Severe acute respiratory syndrome coronavirus 2 (SARS-CoV-2) and coronavirus disease-2019 (COVID-19): the epidemic and the challenges. Int J Antimicrob Agents 2020;55:105924.
14. Huang C, Wang Y, Li X, et al. Clinical features of patients infected with 2019 novel coronavirus in Wuhan, China. Lancet 2020;395:497–506.
15. Guo J, Huang Z, Lin L, Lv J. Coronavirus disease 2019 (COVID-19) and cardiovascular disease: a viewpoint on the potential influence of angiotensin-converting enzyme inhibitors/angiotensin receptor blockers on onset and severity of severe acute respiratory syndrome coronavirus 2 infection. J Am Heart Assoc 2020; 9:e016219.
16. Kalil AC. Treating COVID-19—off-label drug use, compassionate use, and randomized clinical trials during pandemics. JAMA 2020;323:1897–1898.
17. Kappadan V, Telele S, Uzelac I, et al. High-resolution optical measurement of cardiac restitution, contraction, and fibrillation dynamics in beating vs. blebbistatin-uncoupled isolated rabbit hearts. Front Physiol 2020;11:464.
18. Uzelac I, Ji YC, Hornung D, et al. Simultaneous quantification of spatially discordant alternans in voltage and intracellular calcium in Langendorff-perfused rabbit hearts and inconsistencies with models of cardiac action potentials and ca transients. Front Physiol 2017;8:819.
19. Livshitz LM, Rudy Y. Regulation of Ca2+ and electrical alternans in cardiac myocytes: role of CAMKII and repolarizing currents. Am J Physiol Heart Circ Physiol 2007;292:H2854–H2866.
20. O'Hara T, Virág L, Varró A, Rudy Y. Simulation of the undiseased human cardiac ventricular action potential: model formulation and experimental validation. PLoS Comput Biol 2011;7:e1002061.
21. Kaboudian A, Cherry EM, Fenton FH. Real-time interactive simulations of large-scale systems on personal computers and cell phones: toward patient-specific heart modeling and other applications. Sci Adv 2019;5:eaav6019.
22. Bartocci E, Cherry EM, Glimm J, Grosu R, Smolka SA, Fenton FH. Toward real-time simulation of cardiac dynamics. In Proc 9th Int Conf Computational Methods in Systems Biology 2011;103–112.
23. Kashiura M, Fukushima F, Tamura H, Moriya T. T-wave alternans: a harbinger of polymorphic ventricular tachycardia. Oxf Med Case Reports 2019;2019:omz095.
24. Pastore JM, Girouard SD, Laurita KR, Akar FG, Rosenbaum DS. Mechanism linking T-wave alternans to the genesis of cardiac fibrillation. Circulation 1999; 99:1385–1394.
25. Watanabe MA, Fenton FH, Evans SJ, Hastings HM, Karma A. Mechanisms for discordant alternans. J Cardiovasc Electrophysiol 2001;12:196–206.
26. Uzelac I, Iravanian S, Ashikaga H, et al. Fatal arrhythmias: another reason why doctors remain cautious about chloroquine/hydroxychloroquine for treating covid-19. Heart Rhythm 2020;17:1445–1451.
27. Jaeger KH, Edwards AG, McCulloch A, Tveito A. Properties of cardiac conduction in a cell-based computational model. PLoS Comput Biol 2019; 15:e1007042.
28. Delaunois A, Abernathy M, Anderson WD, et al. Applying the CiPA approach to evaluate cardiac proarrhythmia risk of some antimalarials used off-label in the first wave of COVID-19. Clin Transl Sci 2021;14:1133–1146.
29. Sánchez-Chapula JA, Salinas-Stefanon E, Torres-Jácome J, Benavides-Haro DE, Navarro-Polanco RA. Blockade of currents by the antimalarial drug chloroquine in feline ventricular myocytes. J Pharmacol Exp Ther 2001; 297:437–445.
30. Wang G, Tian X, Lu CJ, et al. Mechanistic insights into ventricular arrhythmogenesis of hydroxychloroquine and azithromycin for the treatment of COVID-19. bioRxiv 2020.
31. Walker ML, Rosenbaum DS. Repolarization alternans: implications for the mechanism and prevention of sudden cardiac death. Cardiovasc Res 2003; 57:599–614.
32. Verrier RL, Kumar K, Nearing BD. Basis for sudden cardiac death prediction by T-wave alternans from an integrative physiology perspective. Heart Rhythm 2009;6:416–422.
33. Giudicessi JR, Ackerman MJ. Azithromycin and risk of sudden cardiac death: guilty as charged or falsely accused? Cleve Clin J Med 2013;80:539.
34. Thomsen MB, Beekman J, Attevelt N, et al. No proarrhythmic properties of the antibiotics moxifloxacin or azithromycin in anaesthetized dogs with chronic-AV block. Br J Pharmacol 2006;149:1039–1048.
35. Hondeghem L, Carlsson L, Duker G. Instability and triangulation of the action potential predict serious proarrhythmia, but action potential duration prolongation is antiarrhythmic. Circulation 2001;103:2004–2013.
36. Cherry EM, Fenton FH. Suppression of alternans and conduction blocks despite steep APD restitution: electrotonic, memory, and conduction velocity restitution effects. Am J Physiol Heart Circ Physiol 2004;286:H2332–H2341.
37. Quach B, Krogh-Madsen T, Entcheva E, Christini DJ. Light-activated dynamic clamp using IPSC-derived cardiomyocytes. Biophys J 2018;115:2206–2217.
38. Belardinelli L, Antzelevitch C, Vos MA. Assessing predictors of drug-induced torsade de pointes. Trends Pharmacol Sci 2003;24:619–625.
39. Bryant SM, Wan X, Shipsey SJ, Hart G. Regional differences in the delayed rectifier current (IKr and IKs) contribute to the differences in action potential duration in basal left ventricular myocytes in guinea-pig. Cardiovasc Res 1998;40:322–331.
40. Qu Z, Xie Y, Garfinkel A, Weiss JN. T-wave alternans and arrhythmogenesis in cardiac diseases. Front Physiol 2010;1:154.
41. Armoundas AA, Tomaselli GF, Esperer HD. Pathophysiological basis and clinical application of T-wave alternans. J Am Coll Cardiol 2002;40:207–217.
42. Weiss JN, Garfinkel A, Karagueuzian HS, Chen PS, Qu Z. Early afterdepolarizations and cardiac arrhythmias. Heart Rhythm 2010;7:1891–1899.
43. Samuel S, Friedman RA, Sharma C, et al. Incidence of arrhythmias and electrocardiographic abnormalities in symptomatic pediatric patients with PCR-positive SARS-CoV-2 infection, including drug-induced changes in the corrected QT interval. Heart Rhythm 2020;17:1960–1966.
44. Sicouri S, Quist M, Antzelevitch C. Evidence for the presence of M cells in the guinea pig ventricle. J Cardiovasc Electrophysiol 1996;7:503–511.
45. Drouin E, Charpentier F, Gauthier C, Laurent K, Le Marec H. Electrophysiologic characteristics of cells spanning the left ventricular wall of human heart: evidence for presence of M cells. J Am Coll Cardiol 1995;26:185–192.

46. Osadchii OE. Dofetilide promotes repolarization abnormalities in perfused guinea-pig heart. Cardiovasc Drug Ther 2012;26:489–500.
47. Osadchii OE. Quinidine elicits proarrhythmic changes in ventricular repolarization and refractoriness in guinea-pig. Can J Physiol Pharmacol 2013; 91:306–315.
48. Zhang Y, Xiao J, Lin H, et al. Ionic mechanisms underlying abnormal QT prolongation and the associated arrhythmias in diabetic rabbits: a role of rapid delayed rectifier K+ current. Cell Physiol Biochem 2007;19:225–238.
49. Colatsky T, Fermini B, Gintant G, et al. The comprehensive in vitro proarrhythmia assay (CiPA) initiative—update on progress. J Pharmacol Toxicol Methods 2016; 81:15–20.
50. Koller ML, Maier SK, Gelzer AR, Bauer WR, Meesmann M, Gilmour RF Jr. Altered dynamics of action potential restitution and alternans in humans with structural heart disease. Circulation 2005;112:1542–1548.
51. Lee P, Calvo CJ, Alfonso-Almazán JM, et al. Low-cost optical mapping systems for panoramic imaging of complex arrhythmias and drug-action in translational heart models. Sci Rep 2017;7:1–14.
52. Zeng J, Laurita KR, Rosenbaum DS, Rudy Y. Two components of the delayed rectifier K+ current in ventricular myocytes of the guinea pig type: theoretical formulation and their role in repolarization. Circ Res 1995; 77:140–152.
53. Li GR, Feng J, Yue L, Carrier M, Nattel S. Evidence for two components of delayed rectifier K+ current in human ventricular myocytes. Circ Res 1996;78:689–696.
54. Hondeghem L, Katzung B. Antiarrhythmic agents: the modulated receptor mechanism of action of sodium and calcium channel-blocking drugs. Annu Rev Pharmacol Toxicol 1984;24:387–423.
55. Hondeghem L. Antiarrhythmic agents: modulated receptor applications. Circulation 1987;75:514–520.